약학석사 학위논문

Structural analyses of Ser/Thr kinase HASPIN in complex with nucleoside analogue inhibitors

Ser/Thr 인산화효소 HASPIN과 뉴클레오사이드 유사 저해제 복합체의 구조적 분석

2023년 2월

서울대학교 대학원

약학과 약학전공

서 주 희

Structural analyses of Ser/Thr kinase HASPIN in complex with nucleoside analogue inhibitors

지도 교수 한 병 우

이 논문을 약학석사 학위논문으로 제출함
2022년 11월

서울대학교 대학원
약학과 약학전공
서 주 희

서주희의 약학석사 학위논문을 인준함
2022년 12월

위 원 장 _____ (인)

부위원장 _____ (인)

위 원 _____ (인)

Abstract

HASPIN is a Ser/Thr kinase that plays a critical role in regulating mitosis by phosphorylating the Thr3 of histone H3 at the beginning of mitosis. The phosphorylated histone H3 provides a docking site for the Chromosomal Passenger Complex (CPC) and guide CPC to the centromeric region of the chromosome, so the CPC can work as the master regulator of the cell cycle. As HASPIN is deeply involved in cell cycle regulation, HASPIN has been considered a potential target for anti-cancer therapeutics. However, the atypical kinase structure of HASPIN made it difficult to develop a novel HASPIN inhibitor as the Asp-Phe-Gly (DFG) domain which is critical to the kinase inhibitors is replaced into the Asp-Tyr-Thr (DYT) domain.

In this research, the structure of the HASPIN kinase domain in complex with novel nucleoside analogue inhibitors LJ4827 and LJ4760 are identified in the resolution of 2.70 Å and 2.18 Å respectively using X-ray diffraction. LJ4827 and LJ4760 were both bound at the ATP binding region of the HASPIN kinase domain. The interaction between the inhibitor and the HASPIN hinge region was similar in both inhibitors. However, the interaction between the HASPIN backbone and the moiety of the inhibitor which replaces the hydroxyl group at the 5’ of ribose differed very much. The amino group of LJ4760 interacted with the carbonyl backbone of Gly492 which tilted the phenyl ring of Phe495 outward and the tilting of the phenyl ring is suspected to affect the binding of the substrate.

주요어 : HASPIN, kinase, nucleoside analogue inhibitor, anti-cancer agent

학 번 : 2021-24523

Table of Contents

List of Tables

List of Figures

Introduction

As uncontrolled cell proliferation is the driving force of tumorigenesis and the hallmark of cancer [1], the machineries involved in progressing the cell cycle have been considered a classical target for anti-cancer therapeutics [2, 3]. However, the anti-cancer therapeutics targeting the cell cycle leads to inevitable side effects in highly proliferating tissues such as hair follicles and bone marrow [4, 5].

HASPIN(Haploid germ cell-specific nuclear protein kinase) is a Ser/Thr kinase encoded by the gene GSG2 and its only known substrate so far is the Thr3 of histone H3[6]. The phosphorylated Thr3 of histone H3 (H3T3ph) provides a docking site to the Chromosomal Passenger Complex (CPC)[7], and leads CPC to localize at the centromeric region of the chromosome [8]. Moreover, a positive loop is created by the Aurora B kinase, which is the component of CPC, and participates in further activation of HASPIN [9]. CPC is known as the master regulator of cell division, which regulates the chromosomal structure, kinetochore-microtubule attachment, and spindle assembly at the beginning of mitosis[10]. HASPIN depletion caused mitotic spindle anomalies and a decrease in growth rate, however, it did not abort the cell divisions completely[11]. Inhibition of HASPIN ceased the tumor growth [12], however, HASPIN knock-out mice developed normally without any remarkable change in phenotype or weight except for germ cell disorder[13].

The typical eukaryotic protein kinase (ePK) is composed of two lobes, and the ATP binding domain is located at the deep cleft between the two lobes. The substrate bind at the activation loop, which begins with a highly conserved Asp-Phe-Gly(DFG) motif and ends with Ala-Pro-Glu(APE) motif. The DFG motif is crucial to the function of kinase as it coordinates the Mg^{2+} and ATP. Therefore, the position

of DFG decides the active (DFG-in) and inactive (DFG-out) conformation of an ePK. The protein kinase inhibitors are classified into 4 types, type I and II bind at the ATP binding domain and type III and IV bind at the allosteric region. Most of the protein kinase inhibitors are classified as type I and II. Type I inhibitors bind at the active (DFG-in) position and type II inhibitors bind at the inactive (DFG-out) position of a kinase [14]. HASPIN is classified as an atypical ePK, indicating that the structure of HASPIN kinase domain differs from the typical structure of ePK. Especially the Asp-Phe-Gly(DFG) motif is replaced with the Asp-Tyr-Thr(DYT) motif and the APE motif is missing [15]. As the DFG motif is critical to the binding of kinase inhibitors, the distinct features of HASPIN kinase domain made it difficult to develop a novel HASPIN inhibitor.

Novel nucleoside inhibitors LJ4827 and LJ4760 have been identified by computational analysis. In this research, the structure of HASPIN kinase domain in complex with nucleoside analogue inhibitor LJ4827 and LJ4760 are identified in the resolution of 2.18 Å and 2.70 Å respectively by X-ray diffraction. A docking study was conducted to compare the binding mode and the binding affinity of LJ4827 to LJ4760, 5-iodotubercidin, and CHR6494.

Materials and Methods

1. Cloning and Expression

The Human *HASPIN* clone was provided from Korea Human Gene Bank, Medical Genomics Research center, KRIBB, Korea. The kinase domain of human HASPIN (452-798) was amplified using PCR and cloned into the pET-21a(+) vector (Novagen, Madison, WI, USA). The recombinant plasmid was transformed into Rosetta2(DE3)pLysS (Novagen, Madison, WI, USA) *Escherichia coli* strain. The transformed cells were grown in Luria Broth media containing ampicillin at 37℃ until OD_{600} reached 0.8 and induced with 0.5 mM isopropyl β-D-1-thiogalactopyranoside (IPTG). Inducted cells were grown at 20℃ for 18 hours. The cloning of HASPIN was conducted by Sang Won Cheon.

2. Purification

The cells were harvested by centrifugation at 6000g for 10 minutes. The cell pellets were resuspended in buffer A (500 mM NaCl, 35 mM imidazole, and 20 mM Tris-HCl at pH 7.5) with 1mM phenylmethanesulfonylfluoride (PMSF) and lysed by sonication. The lysates were centrifuged at 35,000g for 1 hour and the supernatants were filtered with a 0.45 μm filter to remove cell debris. The filtered supernatants were loaded onto a 5 mL HiTrap chelating HP column (GE Healthcare, Chicago, IL, USA) which was pre-charged with Ni^{2+} and equilibrated with buffer A. The loaded HASPIN protein was eluted by increasing the gradient of buffer B (500 mM NaCl, 1 M imidazole, and 20 mM Tris-HCl at pH 7.5). The eluted protein was loaded onto HiLoad 16/600 Superdex 75pg column (GE Healthcare, Chicago, IL, USA) which was equilibrated with buffer C (250 mM NaCl, 1mM 1,4-

Dithiothreitol, 10% Glycerol, and 20 mM Tris at pH 7.5). The purified protein was finally concentrated to 5 mg/mL by using Amicon Ultra-10K centrifugal filter device (Millipore, Billerica, Ma, USA).

3. Crystallization

The concentrated protein was preincubated with the inhibitors LJ4827 and LJ4760 in a molar ratio of 1:3 at 4℃ for 30 minutes. The crystals were grown by the sitting-drop vapor diffusion method for screening and optimization respectively at 22℃. For both LJ4827 and LJ4760, the initial crystals were obtained at the commercial crystallization screening solution containing 0.2 M Ammonium sulfate, 0.1 M Sodium acetate trihydrate at pH 4.6, and 25% (w/v) Polyethylene glycol 4000. Initial crystals were further optimized to obtain the diffraction quality crystals. For LJ4827, the diffraction quality crystals were obtained in the solution containing 23.75% (w/v) PEG 4000, 0.2 M ammonium sulfate, and 0.1 M sodium acetate at pH 4.6. For LJ4760, the diffraction quality crystals were obtained in the solution containing 23.75% (w/v) PEG 4000, 0.325 M ammonium sulfate, and 0.1 M sodium acetate at pH 4.6.

4. X-ray data collection

The crystals were cryoprotected in the crystallization solution supplemented with 30% glycerol and flash-frozen in liquid nitrogen. The X-ray diffraction data were obtained at Eiger 9M detector (Dectris Ltd., Baden, Switzerland) at beamline 5C of Pohang Light Source, Korea. For the crystal in complex with LJ4827, the crystal was rotated through a total of 250˚ with a 1.0˚ oscillation range per frame. For the crystal in complex with LJ4760, the crystal was rotated through a

total of 250˚ with a 1.0˚ oscillation range per frame.

5. Structure determination and refinement

The data collected by the synchrotron were processed and scaled using the HKL2000 program suite[16]. The structures were determined by the molecular replacement with the Phaser-MR in PHENIX[17] using the crystal structure of the HASPIN kinase domain (PDB ID: 2WB8) as a phasing model. The model was completed using iterative cycles of model building with Coot[18] and refinement with phenix.refine in PHENIX[17].

6. Docking studies

Autodock Vina[19] was used for the docking studies. HASPIN structure in complex with LJ4827 were used as control and the grid box sized with 10×10×10 points was centered at the LJ4827 binding site with 1.0 Å spacing. LJ4760, 5-iodotubercidin, CHR6494 were used as ligands for docking and the structure of the ligand was obtained by PRODRG[20].

Result

1. Cloning

The kinase domain (residues 452-798) of *HASPIN* was amplified using the PCR and was verified by the agarose gel electrophoresis (Figure 1). After the transformation of the recombinant plasmid, it was once again verified by the agarose gel electrophoresis (Figure 2). Gene sequencing was done to finally confirm that the *HASPIN* kinase domain was properly inserted in the expression vector.

Six competent cells were tested for expression and solubility test. Rosetta2 (DE3) and Rosetta 2(DE3)pLysS *Escherichia coli* strain expressed the most soluble protein at 20℃ (Figure 3).

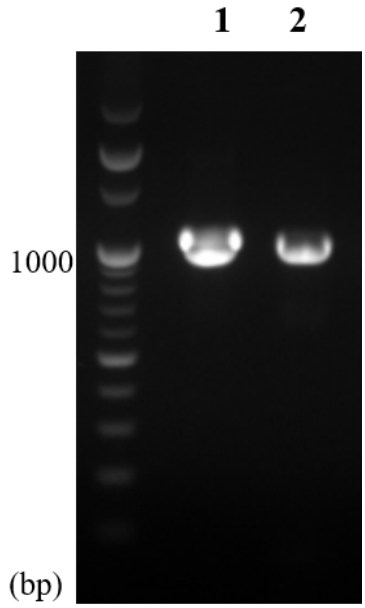

Figure 1. Result of agarose gel electrophoresis after PCR.

Lane 1: *HASPIN* 452-798 no stop codon (1)

Lane 2: *HASPIN* 452-798 no stop codon (2)

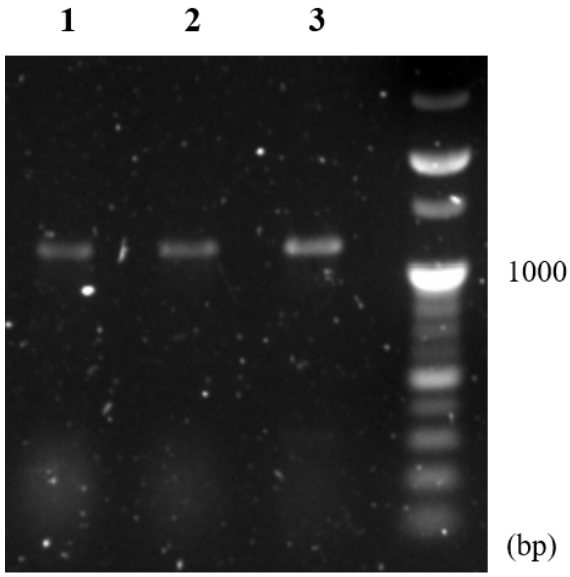

Figure 2. Result of agarose gel electrophoresis after colony PCR.

Lane 1: *HASPIN* 452-798 pET-21a vector (1)

Lane 2: *HASPIN* 452-798 pET-21a vector (2)

Lane 3: *HASPIN* 452-798 pET-21a vector (3)

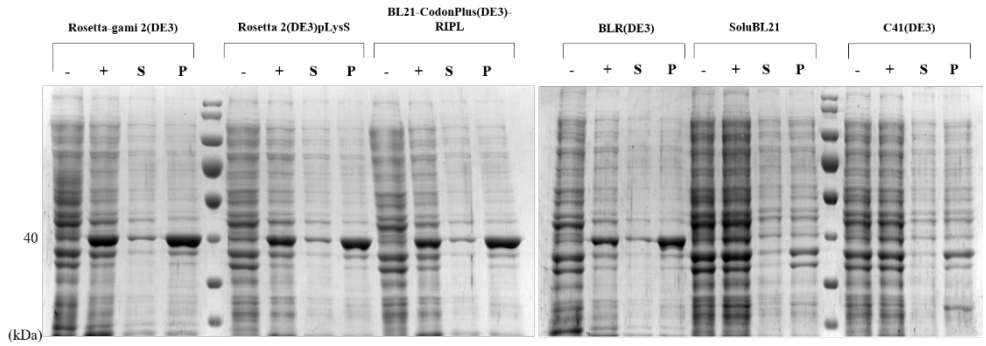

Figure 3. SDS-PAGE analysis after expression test. Rosetta-gami2(DE3), Rosetta2(DE3)pLysS, BL21-CodonPlus(DE3)-RIPL, BLR(DE3), SoluBL21, C41(DE3) *Escherichia coli* cell strains were tested for expression and solubility.

- : Before IPTG induction

+ : After IPTG induction

S : Supernatant

P : Precipitant

2. Purification

The harvested wet cell weight was 14.7g for the 3L culture. The first step utilized the C-terminal hexa-histidine tag by using the Ni^{2+}-chelated HiTrap Chelating HP column (Figure 4). The SDS-PAGE analysis was conducted for the elution fractions from HiTrap Chelating HP column (Figure 5). The eluted proteins were applied to HiLoad 16/600 Superdex 75 pg column (Figure 6). The SDS-PAGE analysis was conducted for the elution fractions from HiLoad 16/600 Superdex 75 pg column (Figure 7).

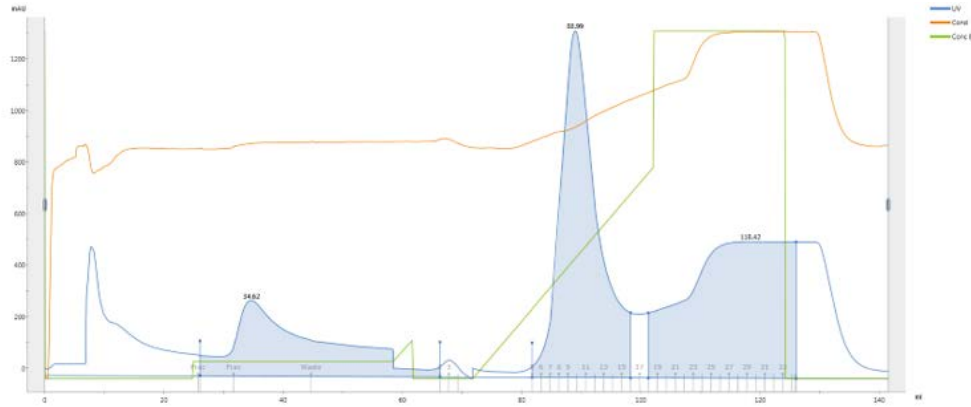

Figure 4. Elution profile from HiTrap Chelating HP column.

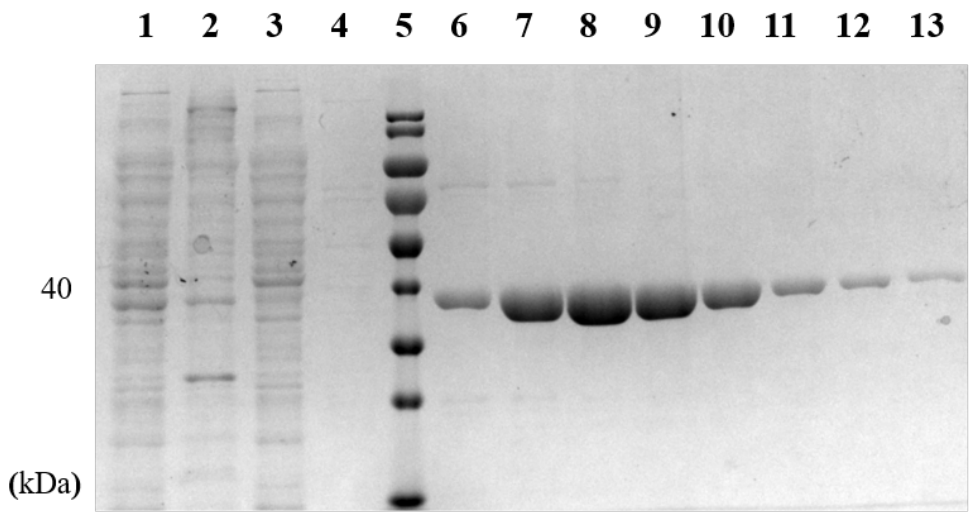

Figure 5. SDS-PAGE analysis for the elution fractions from HiTrap Chelating HP column.

Lane 1:	Sample	Lane 8:	Fraction 9
Lane 2:	Precipitant	Lane 9:	Fraction 10
Lane 3:	Loading through	Lane 10:	Fraction 11
Lane 4:	7% fraction	Lane 11:	Fraction 12
Lane 5:	Protein ladder	Lane 12:	Fraction 13
Lane 6:	Fraction 7	Lane 13:	Fraction 14
Lane 7:	Fraction 8		

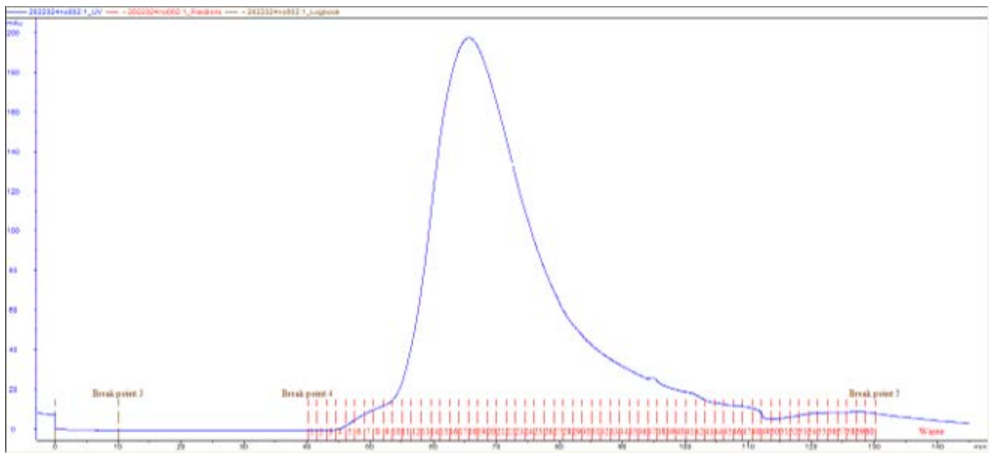

Figure 6. Elution profile from HiLoad 16/600 Superdex 75 pg column.

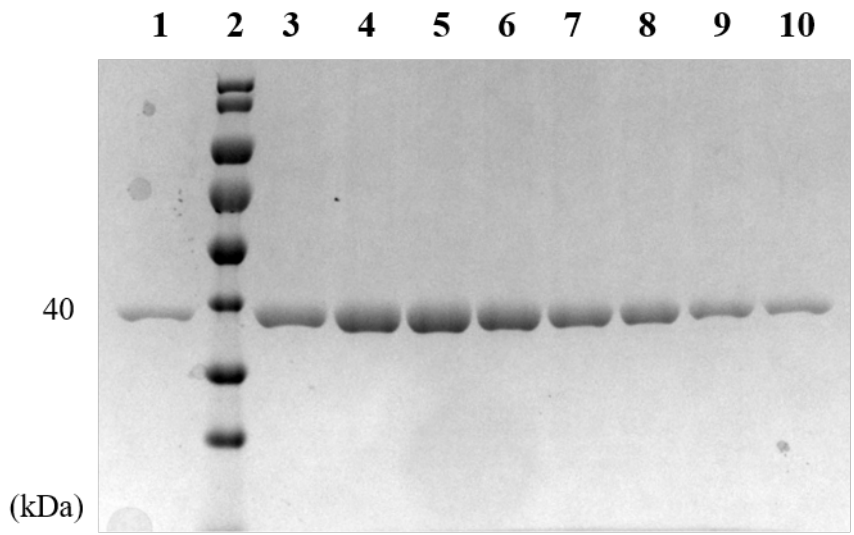

Figure 7. SDS-PAGE analysis for the elution fractions from HiLoad 16/600 Superdex 75 pg column.

Lane 1:	Fraction 12	Lane 6:	Fraction 22
Lane 2:	Fraction 14	Lane 7:	Fraction 24
Lane 3:	Fraction 16	Lane 8:	Fraction 26
Lane 4:	Fraction 18	Lane 9:	Fraction 28
Lane 5:	Fraction 20		

3. Crystallization and X-ray data collection

The crystals of HASPIN in complex with inhibitors LJ4827 and LJ4760 were obtained by sitting drop vapor diffusion method at 22℃ (Figure 8, 9, 10, 11). For LJ4827, the X-ray diffraction data were collected with the optimized crystal and scaled at the resolution of 2.70 Å (Figure 12). For LJ4760, the X-ray diffraction data were collected with the optimized crystal and scaled at the resolution of 2.18 Å (Figure 13). The statistics for the data collection and refinement are summarized in Table 1.

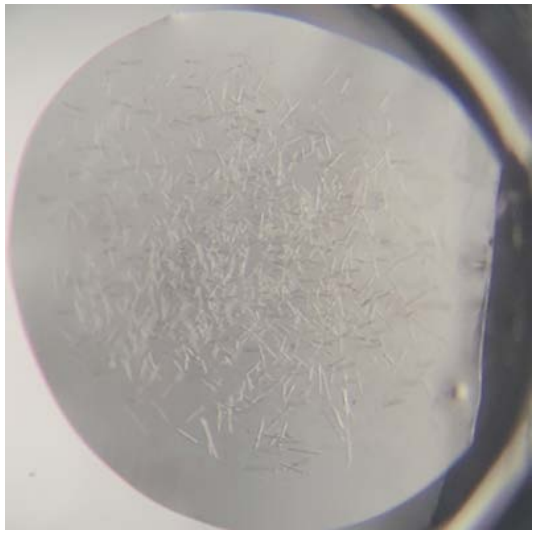

Figure 8. Initial hit crystals of HASPIN in complex with LJ4827.

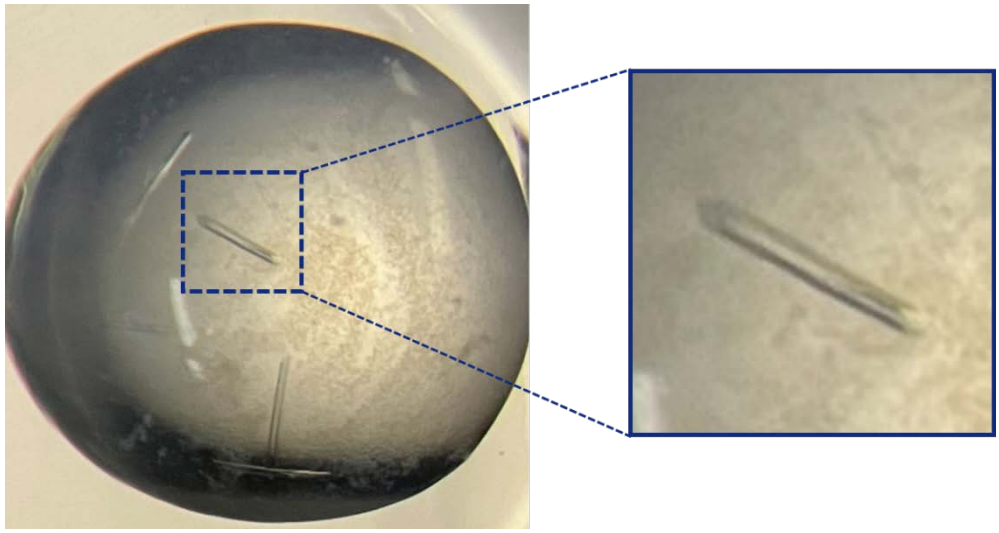

Figure 9. Optimized crystals of HASPIN in complex with LJ4827.

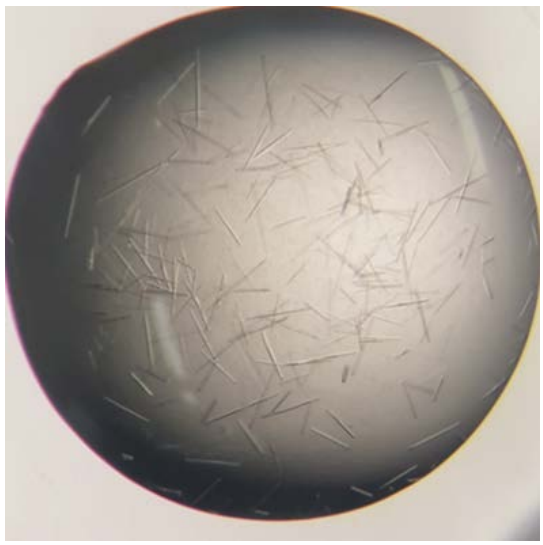

Figure 10. Initial hit crystals of HASPIN in complex with LJ4760.

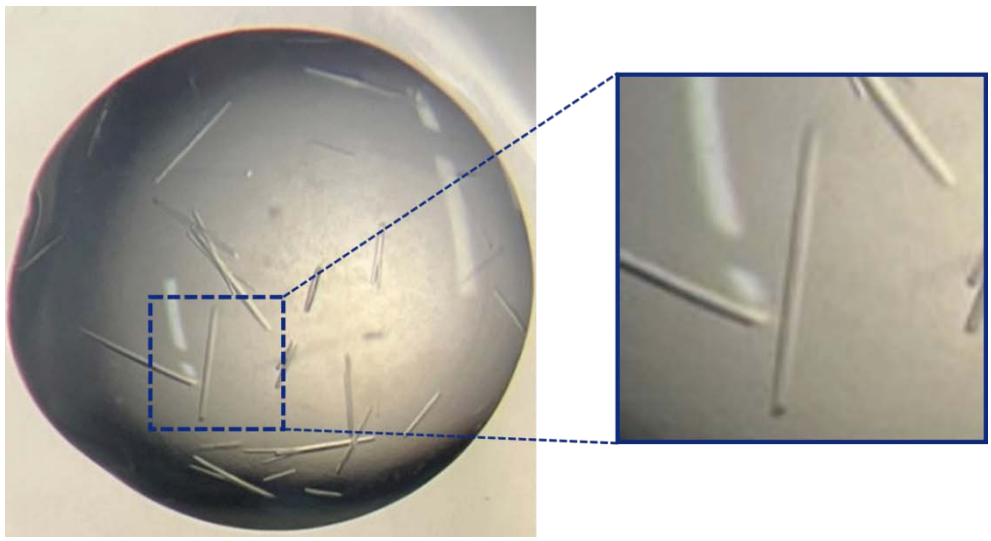

Figure 11. Optimized crystals of HASPIN in complex with LJ4760.

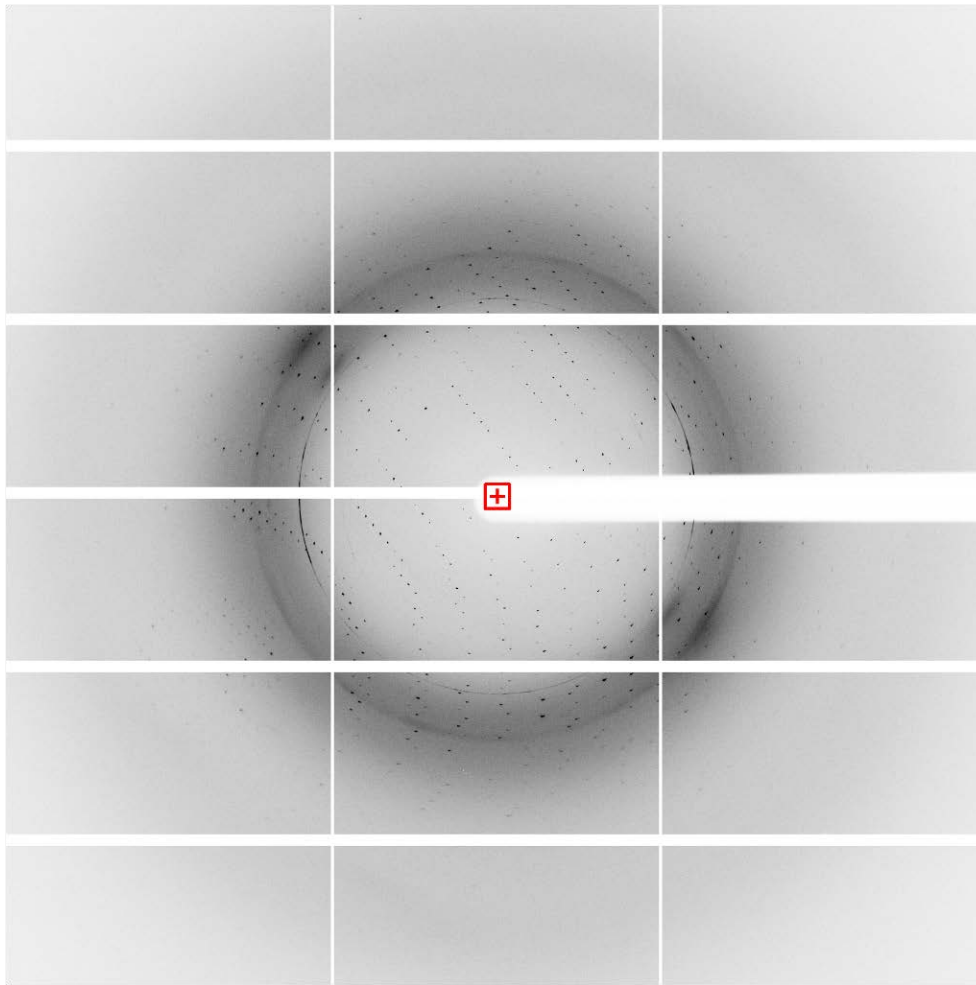

Figure 12. X-ray diffraction data of HASPIN in complex with LJ4827.

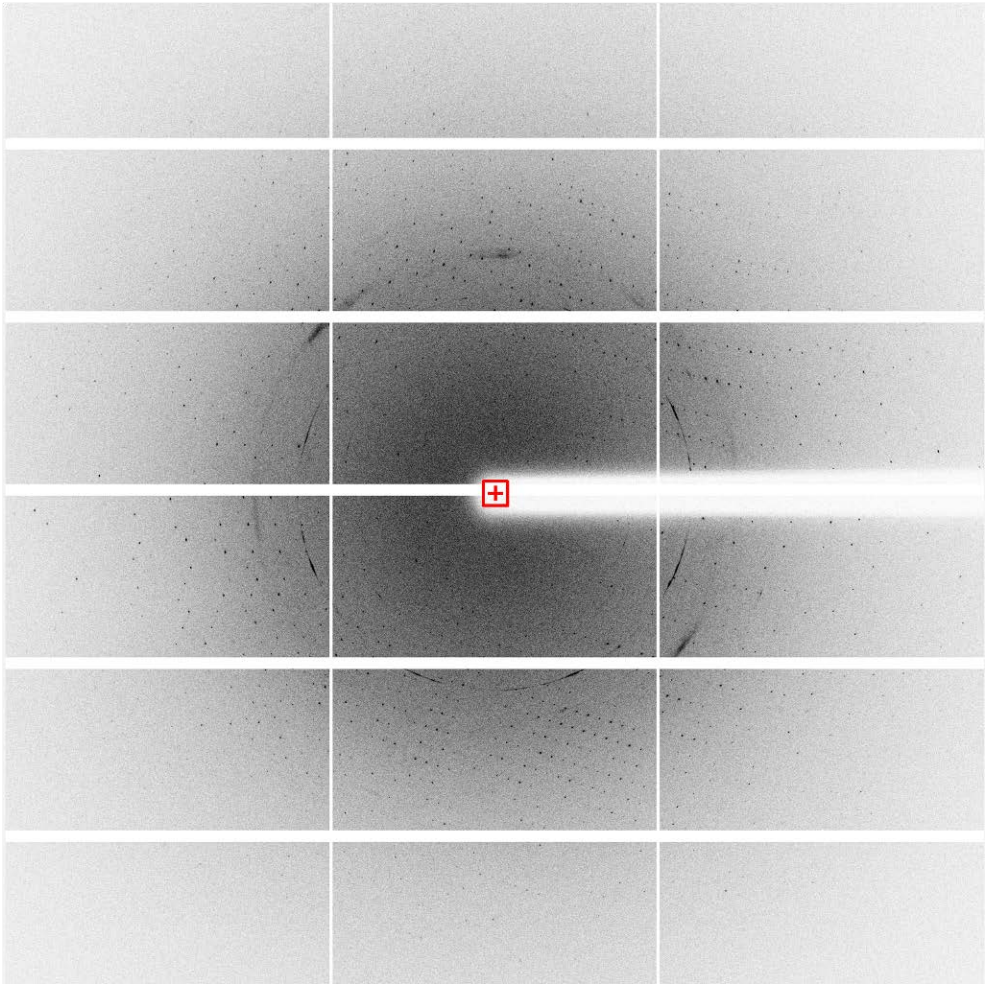

Figure 13. X-ray diffraction data of HASPIN in complex with LJ4760.

	HASPIN + LJ4827	HASPIN + LJ4760
Data collection and phasing		
X-ray source	PLS-5C	PLS-5C
X-ray wavelength (Å)	0.97942	0.97942
Space group	P 2_1 2_1 2_1	P 2_1 2_1 2_1
Unit cell parameters		
a, b, c (Å)	76.854 79.068 82.432	76.263 78.834 82.800
α, β, γ (˚)	90.00 90.00 90.00	90.00 90.00 90.00
Resolution range (Å)	50.00-2.70(2.80-2.70)*	50.00–2.18(2.22-2.18)*
Total/Unique reflection	915556/14296	739456/26745
Redundancy	6.6(6.2)*	8.0(8.2)*
Mean I/σ(I)	18.08(3.27)*	18.15(4.57)*
Completeness (%)	99.09	98.91
R_{merge} (%)	9.7(59.6)*	10.0(47.8)*
$CC_{1/2}$	0.988(0.840)*	1.00(0.918)*
Refinement		
R_{work}/R_{free}	0.1941/0.2290	0.1784/0.2090
No. of non-hydrogen atoms		
Protein	2793	2793
Water	36	122
Mean B value (Å^2)	42.0	33.0
Protein	40.68	32.99
Water	36.46	38.80
Ramachandran plot analysis		
Favored (%)	95.31	98.55
Allowed (%)	4.1	1.45
Disallowed (%)	0.59	0.00
R. m. s. deviations from ideal geometry		
Bond length (Å)	0.007	0.008
Bond angles (˚)	1.03	0.88

*Values in parentheses refer to the last resolution shell

Table 1. Data collection and refinement statistics.

4. The structure of HASPIN kinase domain

The nucleoside analogue inhibitors LJ4827 and LJ4760 were bound at the ATP binding domain of HASPIN kinase domain (Figure 15, 16). The interaction between the inhibitor and HASPIN kinase domain hinge region was similar to that of AMP and 5-iodotubercidin[15]. The N1 and N6 of adenine interacted with Glu606 and Gly608 of the HASPIN hinge region. The 2′ and 3′ hydroxyl groups of ribose interacted with Asp611 and Gly653 of HASPIN (Figure 17).

The difference in interaction with the HASPIN kinase domain was made by the moiety of the ligand which replaces the 5′ hydroxyl group of ribose. In the structure of the HASPIN kinase domain in complex with AMP, the phosphate group at the 5′ of ribose interacted with Lys511. Furthermore, the Lys511 and Asp687 formed a salt-bridge. For 5-iodotubercidin, the hydroxyl group at the 5′ of ribose formed a hydrogen bond with the water which formed a hydrogen bond with Asp687 of HASPIN[15]. In the structure of HASPIN in complex with LJ4827, the azide group did not form any interaction with the HASPIN backbone. However, in the structure of HASPIN in complex with LJ4760, the amino group interacted with the backbone carbonyl group of Glu492. This interaction flipped the phenyl ring of Phe495 outward, which is different from the structure of HASPIN in complex with LJ4827, AMP, and 5-iodotubercidin (Figure 18).

The surface electrostatics visualization generated by APBS(Adaptive Poisson-Boltzmann Solver) showed that by tilting the phenyl ring outward, LJ4760 made an electrostatic hole near the ATP binding domain of HASPIN (Figure 19, 20).

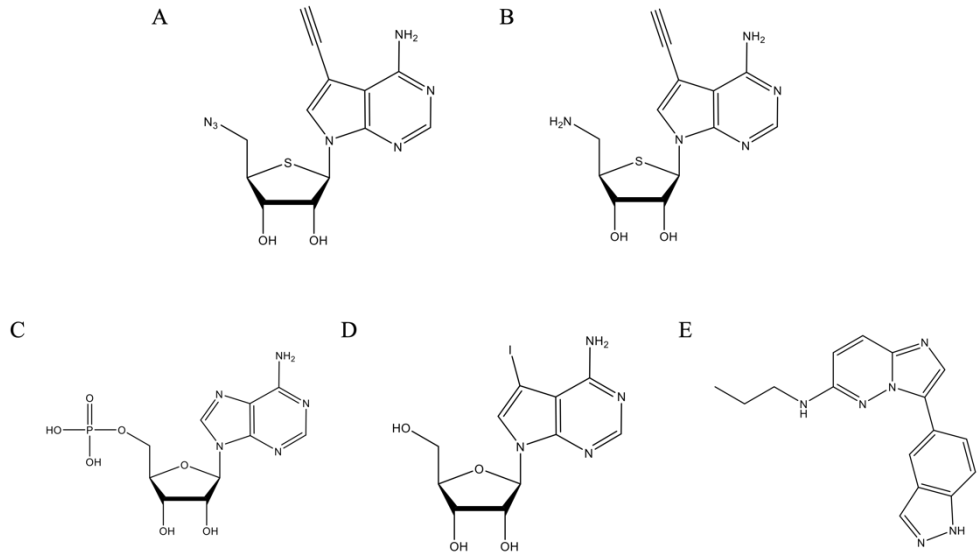

Figure 14. Structure of the ligands. (A) LJ4827 (B) LJ4760 (C) AMP (D) 5-iodotubercidin (E) CHR6494

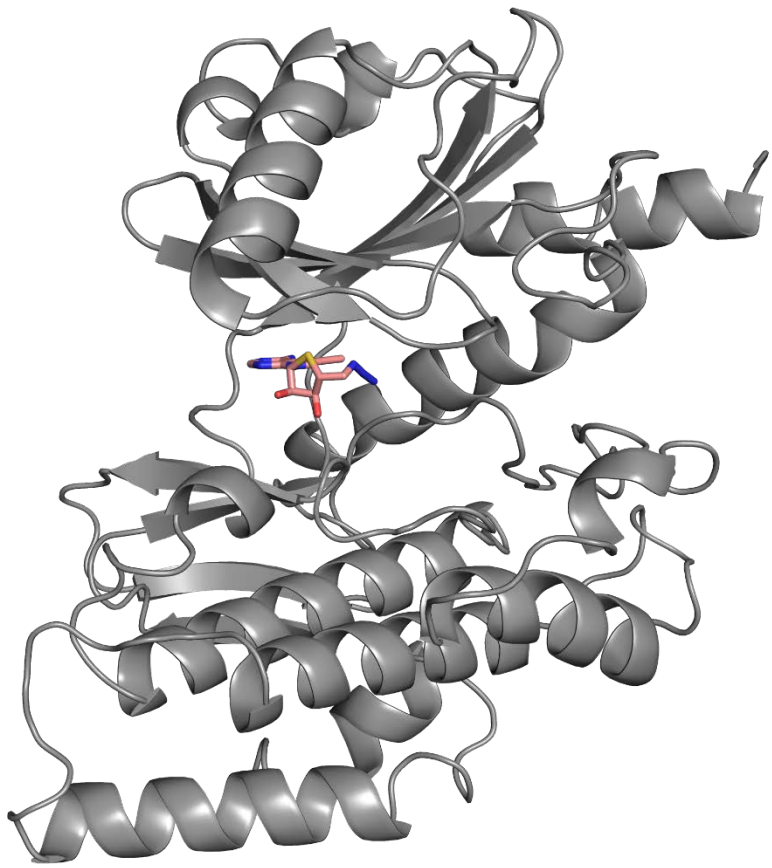

Figure 15. The overall structure of HASPIN kinase domain in complex with LJ4827.

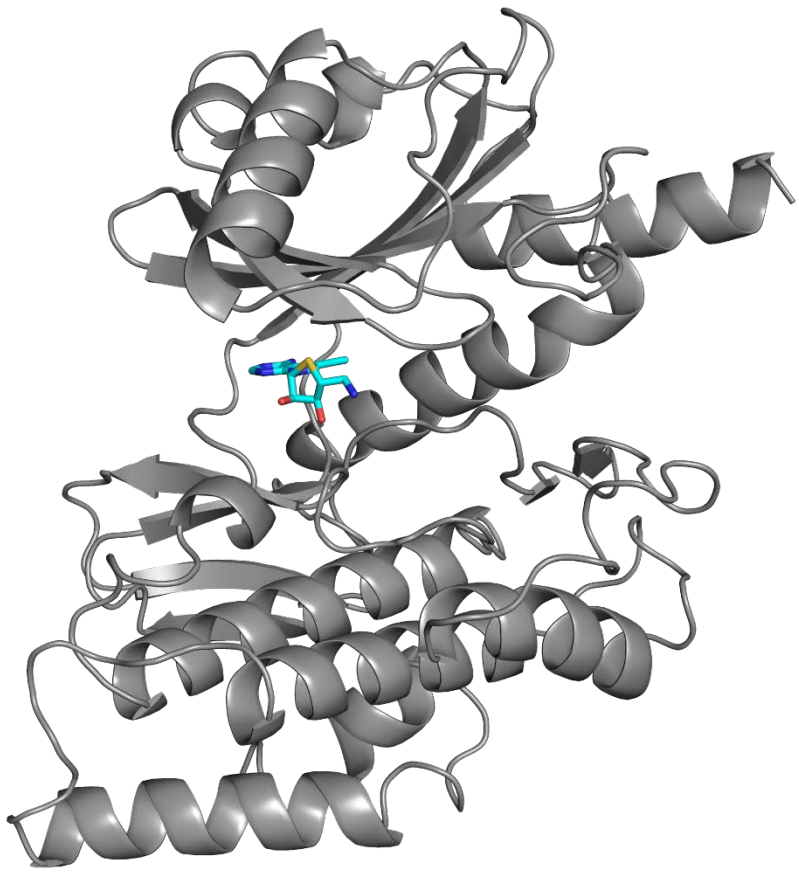

Figure 16. The overall structure of HASPIN kinase domain in complex with LJ4760.

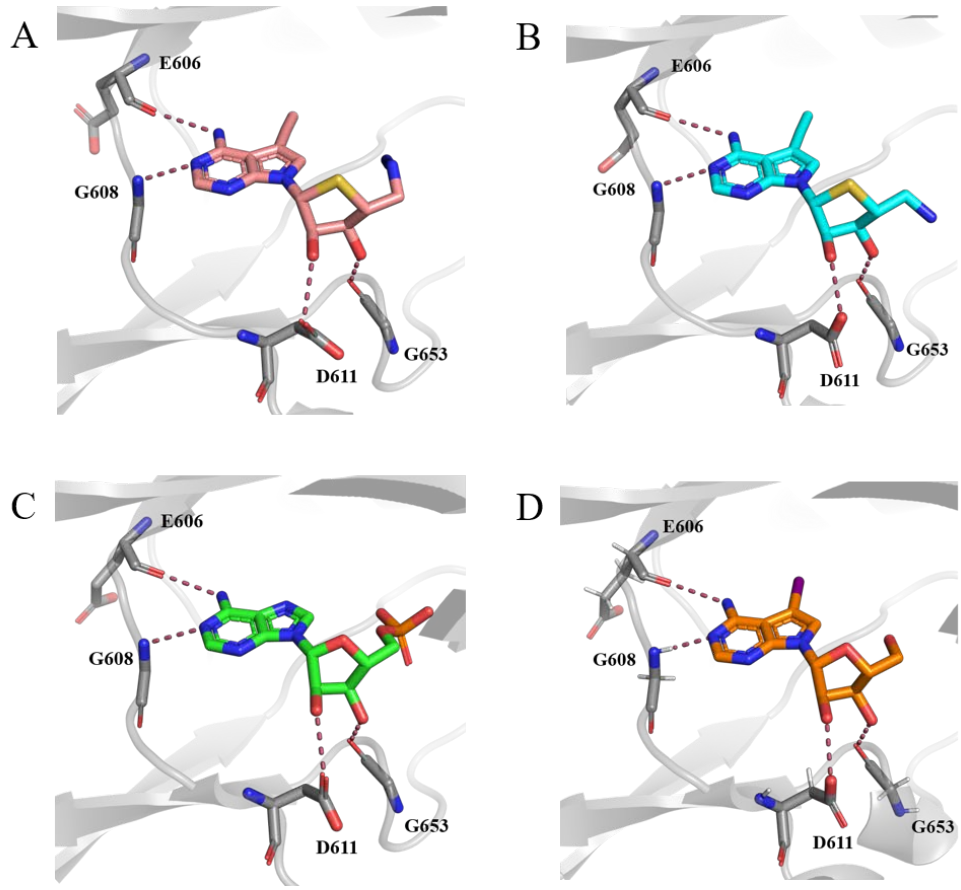

Figure 17. Interaction between the ligand and HASPIN kinase domain hinge region. (A) LJ4827 (B) LJ4760 (C) AMP (PDB ID: 3DLZ) (D) 5-iodotubercidin (PDB ID: 2VUW)

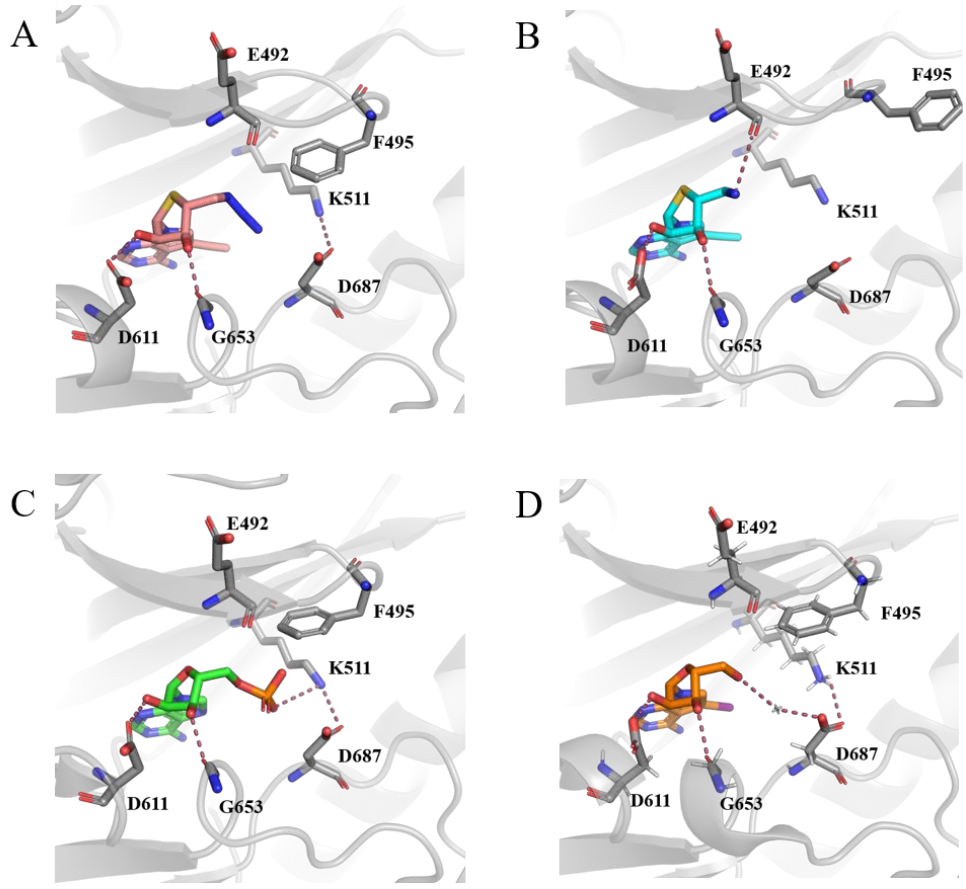

Figure 18. Interaction between the inhibitor moiety which replaces the hydroxyl group on the 5' of ribose and HASPIN kinase domain. (A) LJ4827 (B) LJ4760 (C) AMP (PDB ID: 3DLZ) (D) 5-iodotubercidin (PDB ID: 2VUW)

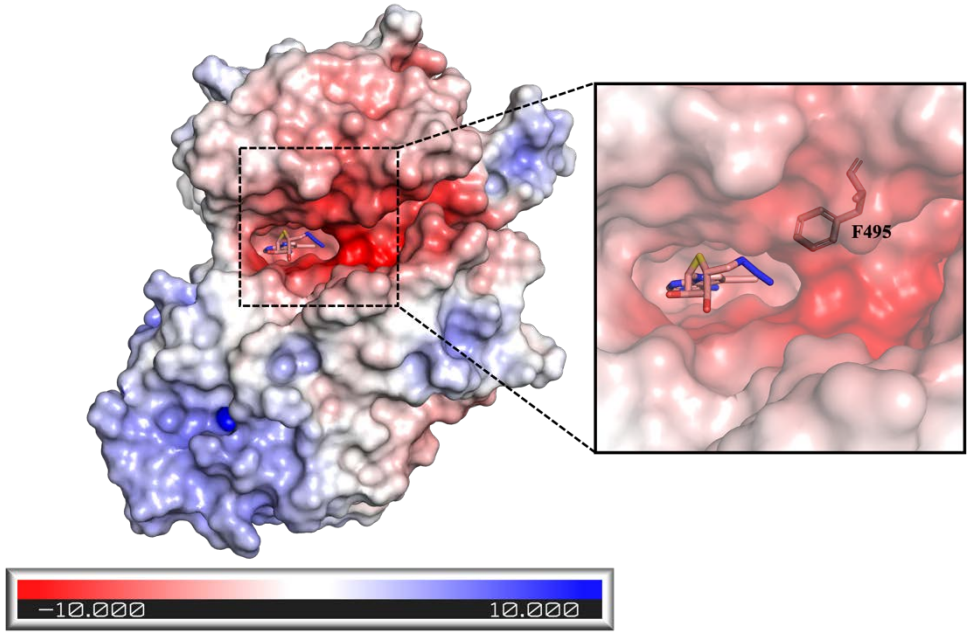

Figure 19. Surface electrostatics visualization by APBS of HASPIN kinase domain in complex with LJ4827.

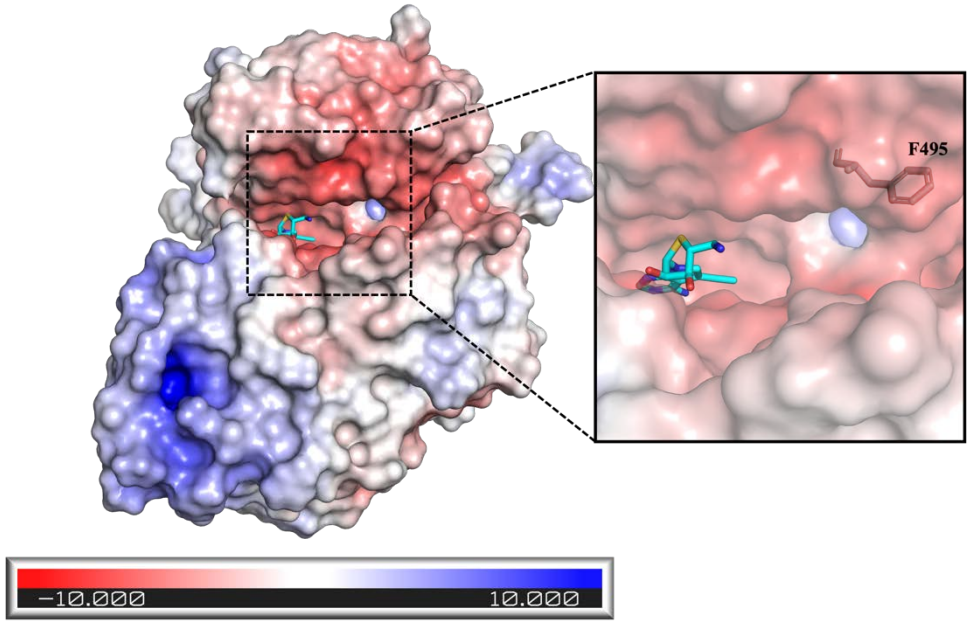

Figure 20. Surface electrostatics visualization by APBS of HASPIN kinase domain in complex with LJ4760.

5. The docking studies

The docking studies were carried out to compare the binding mode and the binding affinity of LJ4827 to other HASPIN inhibitors. The structure of HASPIN in complex with LJ4827 was used as the control and LJ4760, 5-iodotubercidin, and CHR6494 were compared with LJ4827 (Figure 21). The interaction of LJ4827, LJ4760, and 5-iodotubercidin with the HASPIN kinase domain was the same as the identified structure. For CHR6494, the imidazopyridine moiety interacted with Gly608, and the indazole moiety interacted with Lys511 and Asp687 of HASPIN. Of the 4 ligands tested for docking, LJ4827 showed the highest binding affinity (Table 2).

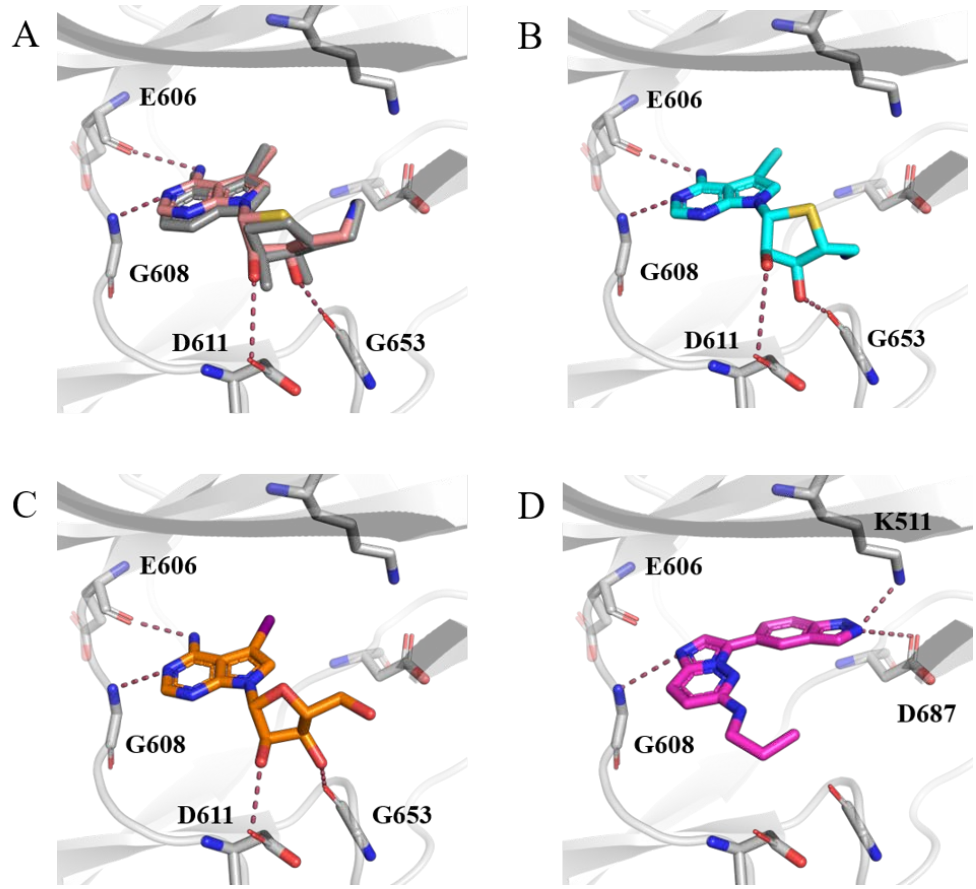

Figure 21. Structures obtained by molecular docking studies. (A) LJ4827(control) (B) LJ4760 (C) 5-iodotubercidin (D) CHR6494.

Inhibitor	LJ4827 (control)	LJ4760	5-iodotubercidin	CHR6494
Affinity (kcal/mol)	-10.3	-8.5	-7.9	-9.9
RMSD	0.522	0.681	0.560	x

Table 2. Binding affinity and RMSD value obtained from the docking studies. The RMSD value refers to the Root mean square deviation (RMSD) value between the identified and molecular docked structures. The Molecular docked structure of LJ4827 was compared with the structure of LJ4827 in complex with HASPIN identified in this research. The Molecular docked structure of LJ4760 was compared with the structure of LJ4760 in complex with HASPIN identified in this research. The molecular docked structure of 5-iodotubercidin was compared with the structure of PDB ID 2VUW. The molecular docked structure of CHR6494 was not able to be compared because the structure of CHR6494 in complex with HASPIN was not identified experimentally.

Discussion

This research identifies the structure of HASPIN in complex with the nucleoside analogue inhibitor LJ4827 and LJ4760. The two nucleoside analogue inhibitors differ only in the moiety that replaces the hydroxyl group on the 5’ of ribose, and it has made a huge difference in interaction with the HASPIN backbone. As shown in figure 19 and 20, the surface electrostatics of HASPIN in complex with LJ4760 showed a positively charged hole adjacent to the ATP binding domain, which did not show in HASPIN in complex with LJ4827, AMP and 5-iodotubercidin. As this hole is located near the activation loop, where the substrate binds, it can be speculated that the tilting of the phenyl might affect the binding of the substrate. Further study of co-crystallizing HASPIN in complex with LJ4760 with Histone H3 peptide must be carried on to prove this hypothesis.

Molecular docking studies were carried on to compare the binding mode and the binding affinity of the HASPIN inhibitors, and LJ4827 showed the highest affinity among the inhibitors compared. In order to back up this result, further studies can be carried on using Isothermal Titration Calometry (ITC) or Surface Plasmon Resonance (SPR).

This research has shown that in nucleoside analogue inhibitors, the moiety which replaces the hydroxyl group at the 5’ of ribose might influence the binding of the substrate. As substrate binding is crucial to a kinase's activity, this result can be used for further development of nucleoside analogue kinase inhibitors.

Bibliography

1. Hanahan, D. and R.A. Weinberg, *Hallmarks of cancer: the next generation.* Cell, 2011. **144**(5): p. 646-74.
2. Williams, G.H. and K. Stoeber, *The cell cycle and cancer.* The Journal of Pathology, 2012. **226**(2): p. 352-364.
3. Otto, T. and P. Sicinski, *Cell cycle proteins as promising targets in cancer therapy.* Nat Rev Cancer, 2017. **17**(2): p. 93-115.
4. Botchkarev, V.A., *Molecular mechanisms of chemotherapy-induced hair loss.* J Investig Dermatol Symp Proc, 2003. **8**(1): p. 72-5.
5. Wang, Y., V. Probin, and D. Zhou, *Cancer therapy-induced residual bone marrow injury-Mechanisms of induction and implication for therapy.* Curr Cancer Ther Rev, 2006. **2**(3): p. 271-279.
6. Dai, J., et al., *The kinase haspin is required for mitotic histone H3 Thr 3 phosphorylation and normal metaphase chromosome alignment.* Genes Dev, 2005. **19**(4): p. 472-88.
7. Jeyaprakash, A.A., et al., *Structural basis for the recognition of phosphorylated histone h3 by the survivin subunit of the chromosomal passenger complex.* Structure, 2011. **19**(11): p. 1625-34.
8. Yamagishi, Y., et al., *Two histone marks establish the inner centromere and chromosome bi-orientation.* Science, 2010. **330**(6001): p. 239-43.
9. Wang, F., et al., *A positive feedback loop involving Haspin and Aurora B promotes CPC accumulation at centromeres in mitosis.* Curr Biol, 2011. **21**(12): p. 1061-9.
10. Carmena, M., et al., *The chromosomal passenger complex (CPC): from easy rider to the godfather of mitosis.* Nat Rev Mol Cell Biol, 2012. **13**(12): p. 789-803.
11. Soupsana, K., et al., *Distinct roles of haspin in stem cell division and male gametogenesis.* Sci Rep, 2021. **11**(1): p. 19901.
12. Huertas, D., et al., *Antitumor activity of a small-molecule inhibitor of the histone kinase Haspin.* Oncogene, 2012. **31**(11): p. 1408-18.
13. Shimada, M., et al., *Essential role of autoactivation circuitry on Aurora B-mediated H2AX-pS121 in mitosis.* Nat Commun, 2016. **7**: p. 12059.
14. Arter, C., et al., *Structural features of the protein kinase domain and targeted binding by small-molecule inhibitors.* J Biol Chem, 2022. **298**(8): p. 102247.
15. Eswaran, J., et al., *Structure and functional characterization of the atypical human kinase haspin.* Proc Natl Acad Sci U S A, 2009. **106**(48): p. 20198-203.
16. Otwinowski, Z. and W. Minor, *Processing of X-ray diffraction data collected in oscillation mode.* Methods Enzymol, 1997. **276**: p. 307-26.
17. Liebschner, D., et al., *Macromolecular structure determination using X-rays, neutrons and electrons: recent developments in Phenix.* Acta

Crystallogr D Struct Biol, 2019. **75**(Pt 10): p. 861-877.
18. Emsley, P., et al., *Features and development of Coot.* Acta Crystallogr D Biol Crystallogr, 2010. **66**(Pt 4): p. 486-501.
19. Trott, O. and A.J. Olson, *AutoDock Vina: improving the speed and accuracy of docking with a new scoring function, efficient optimization, and multithreading.* J Comput Chem, 2010. **31**(2): p. 455-61.
20. Schüttelkopf, A.W. and D.M. van Aalten, *PRODRG: a tool for high-throughput crystallography of protein-ligand complexes.* Acta Crystallogr D Biol Crystallogr, 2004. **60**(Pt 8): p. 1355-63.

국문초록

Ser/Thr 인산화효소 HASPIN과 뉴클레오사이드 유사 저해제 복합체의 구조적 분석

서주희
약학대학 약학 전공
서울대학교 대학원

HASPIN은 Ser/Thr 인산화 효소로 세포분열 초기에 히스톤 H3의 Thr3를 인산화 하여 세포분열의 조절에 주요한 역할을 한다. 인산화 된 히스톤 H3는 Chromosomal Passenger Complex (CPC)에 결합자리를 제공하고, CPC를 염색체의 중심체 부위로 이동시켜 CPC가 세포분열의 마스터 조절자로 작용할 수 있도록 한다. HASPIN은 세포분열에 깊게 연관되어 있는 만큼 항암제의 주요한 타겟으로 여겨져 왔다. 하지만 HASPIN은 인산화 효소 저해제에서 중요한 부분인 Asp-Phe-Gly(DFG)이 Asp-Tyr-Thr(DYT)으로 바뀐 비정형 인산화효소 구조를 가지고 있고, 이러한 구조적 차이로 인해 HASPIN의 저해제 개발에는 어려움이 있었다.

이번 논문에서는 HASPIN 인산화 효소 부위와 새로운 뉴클레오사이드 유사 저해제인 LJ4827과 LJ4760의 콤플렉스 구조를 X-ray

diffraction을 이용하여 각각 2.70 Å과 2.18 Å의 해상도로 규명하였다. LJ4827과 LJ4760은 모두 HASPIN 인산화 효소 부위의 ATP 결합 부위에 결합하였다. HASPIN 경첩 부위와의 상호작용은 두 저해제에서 모두 비슷한 양상을 보였다. 하지만 저해제에서 리보스 5'의 하이드록실기를 대체하는 작용기와 HASPIN과의 상호작용에는 큰 차이가 있었다. LJ4760의 아미노기는 Gly492의 카보닐기와 상호작용하여 Phe495의 페닐기를 바깥쪽으로 기울였고, 기울여진 페닐기가 기질과의 결합에 영향을 주는 것으로 생각된다.

주요어: HASPIN, 인산화 효소, 뉴클레오사이드 유사 저해제, 항암제